Cochlear outer hair cells undergo an apical circumference remodeling constrained by the hair bundle shape.

Raphael Etournay, Léa Lepelletier, Jacques Boutet de Monvel, Vincent Michel, Nadège Cayet, Michel Leibovici, Dominique Weil, Isabelle Foucher, Jean-Pierre Hardelin, Christine Petit

Development 137, 1373-1383 (2010) doi:10.1242/dev.045138

Cochlear outer hair cells undergo an apical circumference remodeling constrained by the hair bundle shape

Raphaël Etournay[1,2,*], Léa Lepelletier[1,3,*], Jacques Boutet de Monvel[1,4], Vincent Michel[1], Nadège Cayet[5], Michel Leibovici[1,6], Dominique Weil[1], Isabelle Foucher[1,7], Jean-Pierre Hardelin[1] and Christine Petit[1,4,†]

SUMMARY

Epithelial cells acquire diverse shapes relating to their different functions. This is particularly relevant for the cochlear outer hair cells (OHCs), whose apical and basolateral shapes accommodate the functioning of these cells as mechano-electrical and electromechanical transducers, respectively. We uncovered a circumferential shape transition of the apical junctional complex (AJC) of OHCs, which occurs during the early postnatal period in the mouse, prior to hearing onset. Geometric analysis of the OHC apical circumference using immunostaining of the AJC protein ZO1 and Fourier-interpolated contour detection characterizes this transition as a switch from a rounded-hexagon to a non-convex circumference delineating two lateral lobes at the neural side of the cell, with a negative curvature in between. This shape tightly correlates with the 'V'-configuration of the OHC hair bundle, the apical mechanosensitive organelle that converts sound-evoked vibrations into variations in cell membrane potential. The OHC apical circumference remodeling failed or was incomplete in all the mouse mutants affected in hair bundle morphogenesis that we tested. During the normal shape transition, myosin VIIa and myosin II (A and B isoforms) displayed polarized redistributions into and out of the developing lobes, respectively, while Shroom2 and F-actin transiently accumulated in the lobes. Defects in these redistributions were observed in the mutants, paralleling their apical circumference abnormalities. Our results point to a pivotal role for actomyosin cytoskeleton tensions in the reshaping of the OHC apical circumference. We propose that this remodeling contributes to optimize the mechanical coupling between the basal and apical poles of mature OHCs.

KEY WORDS: Auditory outer hair cell, Cell shape, Cell-cell junctions, Mechanosensitivity, Hair bundle, Electromotility, Planar polarity, Myosin VIIa, Myosin II, Shroom2, Actin, Cochlear amplifier, Mouse

INTRODUCTION

The importance of the structural and physical properties of cells in relation to their biological functions has long been appreciated (D'Arcy-Thompson, 1961). Only recently, detailed quantitative studies of cell shape have become possible, thanks to improved in vivo and in vitro staining techniques coupled with the growing capabilities of fluorescence microscopy and image processing tools. This is most relevant to the sensory epithelium of the cochlea, the organ of Corti, which comprises various cell types of different shapes and functions. Among these are the auditory hair cells that operate mechano-electrical transduction of incoming sound waves. Each hair cell has a bundle of large and stiff microvilli called stereocilia projecting from the apical cell surface. Deflection of this hair bundle gates transducer channels located at the stereocilia tips (Beurg et al., 2009), whose opening and closure modulate the cell membrane potential, effectively converting the sound-evoked mechanical stimulus into an electrical signal (Fettiplace and Hackney, 2006; Hudspeth, 1989). The cochlea contains two types of hair cells that have markedly different shapes and functions. Inner hair cells (IHCs), organized in one single row, are genuine sensory cells that transmit electric signals to the auditory nerve, whereas outer hair cells (OHCs), organized in three rows, are essential for the amplification of sound-evoked vibrations of the organ of Corti (Dallos et al., 2008). OHCs indeed operate both as mechano-electrical and electromechanical transducers: they convert changes of their membrane potential into mechanical forces and movements directed along their cylindrical cell body (Ashmore, 2008; Brownell et al., 1985). Forces associated with OHC electromotility are believed to feedback energy into the organ of Corti on a cycle-by-cycle basis, thereby amplifying its vibrations in response to low-intensity sounds more than a hundredfold (Dallos, 1992; Fettiplace and Hackney, 2006).

The apices of mature cochlear hair cells and their supporting cells form a regular, tightly joined planar mosaic called the reticular lamina (Fig. 1). Each OHC forms specialized junctions with four supporting cells (Gulley and Reese, 1976). These large hybrid junctions (~3-5 μm in height) are unique in that they combine ultrastructural features of tight junctions and adherens junctions, hence their name of 'tight-adherens junctions' (Nunes et al., 2006). These junctions must fulfil seemingly conflicting mechanical requirements. On the one hand, they undergo substantial mechanical stress imposed by sound-evoked vibrations of the reticular lamina (Tomo et al., 2007), which includes the forces (reaching the nN range) produced by OHC electromotility (Frank et al., 1999; Iwasa and Adachi, 1997; Karavitaki and Mountain, 2007; Mammano and Ashmore, 1993; Nowotny and Gummer, 2006). On the other hand, the auditory system of mammals is sensitive enough to detect sound

[1]Unité de Génétique et Physiologie de l'Audition, Inserm UMRS587-Université Paris VI, Institut Pasteur, 25 rue du Dr Roux, 75724 Paris Cedex 15, France. [2]Max Planck Institute of Molecular Cell Biology and Genetics, Pfotenhauerstrasse-108, 01307 Dresden, Germany. [3]Université Paris VII, Bâtiment des Grands Moulins, 75205 Paris Cedex 13, France. [4]Collège de France, 11 place Marcelin Berthelot, 75231 Paris Cedex 05, France. [5]Plate-Forme de Microscopie Ultrastructurale, Institut Pasteur, 25 rue du Dr Roux, 75724 Paris Cedex 15, France. [6]Département de Biologie du Développement, Institut Pasteur, 25 rue du Dr Roux, 75724 Paris Cedex 15, France. [7]Unité Développement, Evolution, Plasticité du Système Nerveux, CNRS UPR2197-Université Paris XI, Institut de Neurobiologie Alfred Fessard, 91198, Gif-sur-Yvette Cedex, France.

*These authors contributed equally to this work
†Author for correspondence (christine.petit@pasteur.fr)

Accepted 11 February 2010

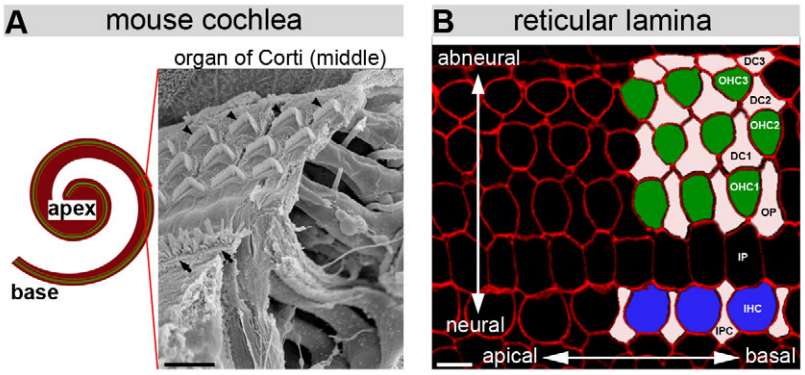

Fig. 1. The mouse auditory organ. (**A**) Left panel: the cochlea, subdivided into three regions: base, middle and apex. Right panel: scanning electron micrograph of a section of the organ of Corti from the middle region. Sensory hair cells [one inner hair cell (IHC) row and three outer hair cell (OHC) rows numbered 1, 2 and 3] are innervated by neurons projecting radially from the central bony core of the cochlea, thus defining the neural-abneural axis of the organ of Corti. The hair bundles of IHCs (arrows) and OHCs (arrowheads) are organized in 3-4 stereocilia rows forming symmetric U- and V-patterns, respectively. They are rigorously positioned with respect to the cochlear baso-apical and neural-abneural axes, thus defining the planar polarity of the cochlear neuroepithelium. The reticular lamina, a stiff plate formed by the apical surfaces of hair cells and their supporting cells, communicates its motion to the hair bundle bases. In addition, the tight junctions between hair cells and supporting cells constitute an ionic barrier separating the K^+-rich endolymph bathing the apices of these cells from the Na^+-rich perilymph bathing their basolateral membranes, a feature crucial for auditory mechanoelectrical transduction (Wangemann, 2006). The morphological, mechanical and physiological properties of the hair cells vary along the cochlear longitudinal axis. These variations underlie the tonotopic organization of the cochlea, i.e. the tuning of hair cells at different cochlear positions to distinct frequencies (Frolenkov et al., 2004; Furness et al., 2008). (**B**) Confocal image of a ZO1-immunostained P0 mouse cochlea showing a top view of the organ of Corti. IHCs make junctions with inner phalangeal cells (IPC) and with one row of inner pillar cells (IP). The OHCs are arranged in a mosaic pattern made of alternating junctions with one row of outer pillar cells (OP) and three rows of Deiters cells (DC1-3). Scale bars: 10 μm in A; 5 μm in B.

power levels barely above thermal noise in magnitude, which corresponds to forces experienced by each hair bundle in the pN range. Indeed, experimental evidence has shown that OHC hair bundles are capable of signaling such small forces in vitro (van Netten et al., 2003). With the bodies of the OHC being free of contact with other cells except at their base and apex, their apical junctional complex (AJC) would be expected to acquire finely adjusted mechanical properties during development for sustaining the large mechanical stresses acting on the reticular lamina, while allowing effective transmission of the small forces acting on the hair bundles at the hearing threshold. Here, driven by the idea that specific signatures at the apical pole of OHCs might accompany the onset of electromotility, we characterized a remodeling of the apical circumference of these cells that occurs during the first postnatal week in the mouse. We studied its relationship with the hair bundle shape, and investigated the associated changes in the distributions of cytoskeleton-associated proteins.

MATERIALS AND METHODS

Animals and antibodies

Wild-type C57BL/6 mice were used for this study. *Myo7a*$^{4626SB/4626SB}$ mice that carry a nonsense mutation in the myosin VIIa motor head were kindly provided by Prof. Karen Steel (Sanger Institute, Cambridge, UK). Harmonin-null mice (Lefèvre et al., 2008) and cadherin 23-null mice (see Fig. S1 in the supplementary material) were produced in collaboration with the Institut Clinique de la Souris (Illkirch, France; Prof. Jean-Louis Mandel). Whirler (*Whrn*$^{wi/wi}$) and shaker 2 (*Myo15a*$^{sh2/sh2}$) mutant mice were kindly provided by Prof. Steve Brown (MRC Harwell, Harwell Science and Innovation Campus, UK) and Prof. Karen Steel, respectively. All animal procedures were carried out in accordance with both INSERM and Pasteur Institute welfare guidelines.

The rabbit polyclonal antibodies used to detect myosin VIIa (1:1000) and Shroom2 (1:100) have been previously described (Boeda et al., 2002; Etournay et al., 2007). The other antibodies are commercially available: rabbit anti-ZO1 (1:100; Zymed), anti-NMHCII A (1:250; Abcam), anti-NMHCII B (1:500; Abcam) and anti-S19phosphoRLC (MYL9; 1:500; Abcam) polyclonal antibodies; mouse anti-E-cadherin, anti-N-cadherin (1:100; BD Biosciences) and anti-ZO1 (1:100; Zymed) monoclonal antibodies; Alexa Fluor 488 F(ab′)2 fragment of goat anti-rabbit IgG, Alexa Fluor 488 F(ab′)2 fragment of goat anti-mouse IgG, (1:500; Molecular Probes-Invitrogen, Cergy Pontoise, France). The MYL9 antibody specifically recognizes the phosphorylated serine 19 of the myosin II regulatory light chain and has been used to detect the pattern of activity of myosin II, irrespective of its isoforms (A, B or C) (Somlyo and Somlyo, 2003). Tetramethyl rhodamine isothiocyanate (TRITC)-conjugated phalloidin (1:1000; Sigma-Aldrich) was used to stain actin filaments.

Wholemount immunofluorescence

Mouse inner ears were rapidly dissected from temporal bones at different developmental stages in HEPES-buffered (10 mM, pH 7.4) Hanks' balanced salts solution. The stria vascularis and the tectorial membrane were removed, and the organ of Corti was immersed either in 4% paraformaldehyde (PFA, 1 hour at room temperature) or cold methanol (10 minutes at –20°C) for fixation. After two washes in phosphate-buffered saline (PBS), the tissue was incubated in 20% normal goat serum for 1 hour (with 0.3% triton for PFA-fixed tissues), and then with the primary antibody at 4°C overnight. After three washes in PBS, samples were incubated with the secondary antibody for 2 hours at room temperature, washed again three times in PBS and mounted in Fluorsave solution (Calbiochem). Fluorescence images were obtained with a confocal microscope (Zeiss LSM 510 META) equipped with a Plan Apochromat 63×/1.4 oil immersion objective. For 3D reconstructions, *z*-stack images were deconvolved and reconstructed with Huygens (Scientific Volume Imaging, Hilversum, The Netherlands) and Imaris (Bitplane Scientific Software) softwares, respectively. 3D OHC models were built using the open source Blender software (http://www.blender.org/).

Transmission electron microscopy

The cochlear shell was pierced at its apex, and the round and oval windows opened. Inner ears were then immersed for fixation in 2% paraformaldehyde plus 2.5% glutaraldehyde in 100 mM sodium cacodylate supplemented with

1% tanic acid for 2 hours at room temperature. Procedures for transmission electron microscopy were as previously described (Goodyear et al., 2005). Images were acquired using a Jeol 1200EX electron microscope.

Hair cell contour detection and geometric characterization

To quantitatively analyze the shape transition of the OHC apical circumference, we used a custom software written in Matlab (The Mathworks), allowing us to semi-automatically extract apical hair cell contours from confocal image stacks of mouse ZO1-stained cochleas. After filtering the images to reduce noise and selecting cells to be processed, an automatic contour extraction was performed based on local maxima detection, which produced a discretized parametrization of the corresponding cell contours (n=100 points in polar coordinates). A continuous polar parametrization was then obtained using a Fourier series interpolation, which allowed us to analyze conveniently the local curvature and various geometric parameters of each contour. The detection algorithm was fast, and accurately delineated the hair cell circumferences on images of variable quality. Prior to averaging, the samples of extracted contours were aligned with respect to the mean contour to compensate for small variations in contour orientation (due mainly to slight differences in image orientation or occasional hair cell misalignment).

The surface area and perimeter of the region enclosed by the contour are denoted by A and P, respectively. From these parameters we deduce the inverse isoperimetric ratio $4\pi A/P^2$, which is unity for a circular contour and less than 1 in all other cases. The contour geometry is fully characterized by its signed curvature K (equivalently, its radius of curvature R=1/K), counted positive at points where the center of curvature is positioned on the side of the interior of the contour, and negative elsewhere. The curvature is obtained from the contour polar parametrization by computing the second derivative of the contour point M with respect to arc-length l, and by using the formula $d^2M/dl^2=Kn$, where n denotes the unit vector normal to the contour at the given point and oriented toward its interior. To quantify the closeness of a contour to being convex, we define its convexity ratio as the ratio $\int Kdl/\int|K|dl$ of the mean signed curvature to the mean of its absolute value. This ratio is unity if the contour as a whole is convex and less than 1 if not.

RESULTS

OHCs adopt a non-convex apical circumference shape during early postnatal development

To study the hair-cell apical circumference shape, fixed and wholemount organs of Corti were stained for the tight junction protein ZO1 (Fanning and Anderson, 2009; Stevenson et al., 1986), which encompasses the entire tight-adherens junctions of OHCs (Nunes et al., 2006). Within the first postnatal week (P1-P7), there was a marked narrowing down of the sensory epithelium along the neural-abneural axis (Fig. 1B, Fig. 2A) extending from the base to the middle of the cochlea, as previously described (Burda and Branis, 1988). In this cochlear region, we detected a concomitant shape change of the OHC apical circumferences, which, from rounded hexagons at the P1 cochlear base, flattened on their neural side at P3 and then switched to a non-convex shape between P3 and P5. This switch could be ascribed to the formation of two lateral lobes flanking a membrane concavity on the OHC neural side (Fig. 2B). Extending approximately up to the basal half of the cochlea at P5, the transition spread over the entire cochlear length at P7, thus following the well-established base-to-apex tonotopic gradient of differentiation in the cochlea (Fritzsch et al., 2006). To characterize this convex to non-convex transition, we carried out a quantitative analysis of the OHC and IHC apical circumferences at the cochlear base. We used custom Matlab software to extract the hair cell contours from confocal images of ZO1-stained cochleas and analyzed geometric parameters computed from the data obtained (see Materials and methods). The convexity ratio of the OHC apical circumference was close to 1 between P1 and P3, but the inverse isoperimetric ratio $4\pi A/P^2$ decreased from ~0.95 at P1 to ~0.88 at P3, indicating a shift from a near-circular to a flattened contour shape (Table 1 in Fig. 2B; see Materials and methods for definitions). This flattening of the neural side, detectable in about 50% of OHCs at P3, was delimited by two points of maximum curvature indicating the emplacements where the lateral lobes would develop. Both the convexity ratio and the $4\pi A/P^2$ ratio displayed maximal decrease between P3 and P5 (Welch's t-test, $P<10^{-6}$ for both ratios). During this period, the OHC apical circumference also adopted a form closer to a triangle, with a base ending in the two lateral lobes and the vertex being associated with the abneural side (Fig. 2B). Shape changes occurring after P5 were less dramatic and consisted mainly in the further development of the lateral lobes, which had attained their adult shape by P7.5. To characterize the negative curvature region of the OHC apical circumference, we defined a reference 'fold angle' delimiting this region (Fig. 2B; see also Fig. S2A in the supplementary material). At P1, all of the OHCs analyzed at the cochlear base (n=164) had an everywhere convex circumference. At P3, a small fraction (<10%) of OHCs displayed a small region of negative curvature (fold angle spanning 5°-30° in OHC rows 1 and 2). At P5, this region was detected in most OHCs (>90%) and covered an angle of about 50°. This angle exhibited little variation from P5 to P7.5. Along with its circumferential shape change, the OHC apical surface area decreased by ~35% between P3 and P5 (Welch's t-test, $P<10^{-9}$), whereas its total decrease over the P1-P7.5 period was of 50-60%. The corresponding decrease in perimeter was ~12% between P3 and P5 (Welch's t-test $P<10^{-7}$), for an ~20% total reduction between P1 and P7.5. Of note, the IHC apical circumference also underwent a transition from a near circular shape at P1 to a rounded rectangular one from P5 on, but remained convex, as shown by a mean convexity ratio greater than 0.95 at all stages.

The formation of a non-convex apical shape in OHCs is striking given that the lateral wall of their cell body just beneath forms a cylinder of near-circular cross-section (Belyantseva et al., 2000; Holley and Ashmore, 1990; Legendre et al., 2008). To investigate the geometry of the junctional region along its apico-basal axis, 3D reconstructions of the ZO1-labeled OHC apical region, based on confocal image stacks scanning the entire AJC, were carried out. At P3, the OHC junctional region, on its entire height, displayed a convex cross-sectional circumference in OHCs (Fig. 3A). At P5, the circumference had become non-convex in its apical part (with a concavity delimited by two not yet very pronounced lateral lobes), whereas it remained convex just below. This conferred a flared aspect to the neural side of the junctional circumference (Fig. 3B). At P7.5, the lower membrane of the fully developed OHC lateral lobes extended nearly parallel to the plane of the reticular lamina, thereby partially overlaying the surface of the adjacent supporting cells and partially underlying the OHC cuticular plate (Fig. 3C).

The cuticular plate is a planar meshwork extending parallel to the apical surface of hair cells and composed mainly of actin filaments (DeRosier and Tilney, 1989). Apart from a small number of 'channels' traversed by microtubules, it appears continuous with a submembrane actin ring that runs the length of the apical junctions (Steyger et al., 1989). Images of cochleas double-stained against F-actin and ZO1 showed that in both hair cell types the cuticular plate remained at all stages delimited by their apical cell circumferences (Fig. 6B; see also Fig. S3A in the supplementary material). As a result, the perimeter of the cuticular plate of OHCs underwent shape changes that closely paralleled those of the cell circumference.

The OHC apical circumference and hair bundle shapes correlate

The near-triangular shape of the OHC apical circumference at mature stages seems to be molded to the 'V'-pattern of the overlying hair bundle. Strikingly, the match in orientation of these two

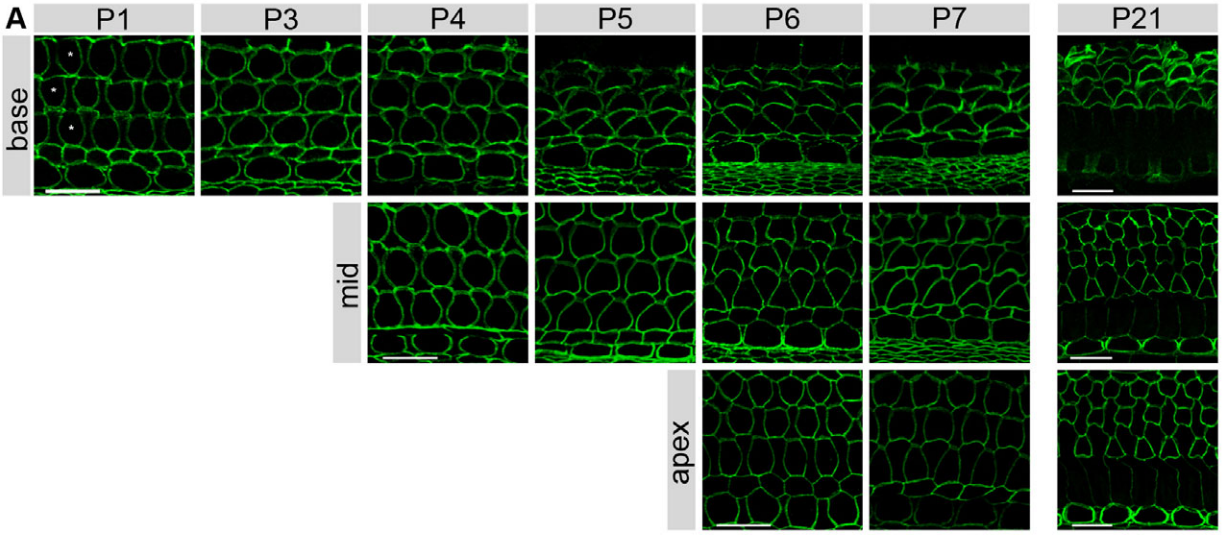

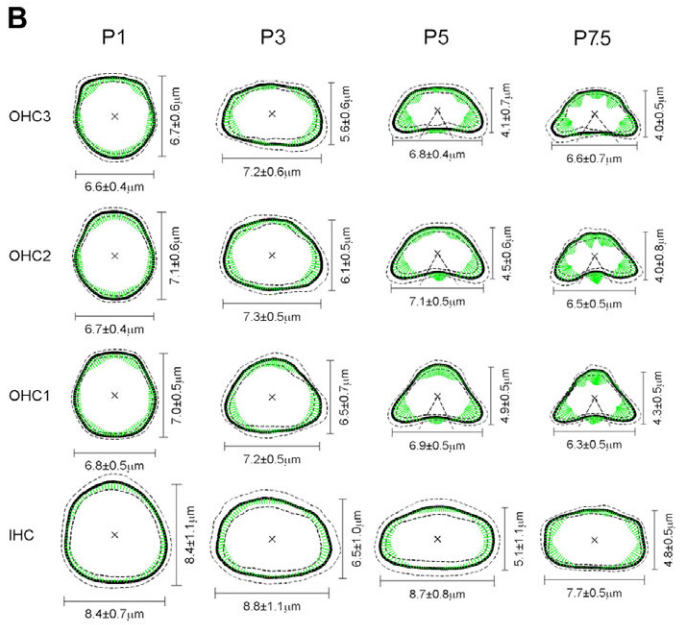

	P1	P3	P5	P7.5
OHC3	n=55	n=19	n=126	n=22
Area (µm²)	34.0 ± 3.79	29.4 ± 4.1**	18.4 ± 3.5***	16.8 ± 1.8*
Perimeter (µm)	21.3 ± 1.29	20.8 ± 1.5	18.1 ± 1.4***	17.3 ± 0.94*
Convexity ratio	1.00 ± 0.00	0.97 ± 0.04*	0.87 ± 0.08***	0.91 ± 0.06*
Ratio 4π A/P²	0.94 ± 0.02	0.85 ± 0.04***	0.70 ± 0.05***	0.70 ± 0.07
% OHC fold	0%	37%	91.3%	95.5%
Fold angle (°)	0	12.3 ± 16.9*	55.7 ± 28.1***	49.3 ± 27.1
Fold radius (µm)	-	-8.4 ± 4.7	-4.9 ± 3.2	-6.29 ± 3.8
% OHC base	0%	68%	100%	100%
Lobes radius (µm)	-	2.4 ± 0.2	1.95 ± 0.2**	1.87 ± 0.16
OHC2	n=55	n=22	n=118	n=23
Area (µm²)	35.5 ± 3.1	32.5 ± 2.5**	20.5 ± 3.5***	15.8 ± 2.9***
Perimeter (µm)	21.8 ± 1.04	21.5 ± 1.3	19.1 ± 1.5***	17.1 ± 1.5**
Convexity ratio	1.00 ± 0.00	0.99 ± 0.02*	0.82 ± 0.09***	0.79 ± 0.06
Ratio 4π A/P²	0.94 ± 0.02	0.88 ± 0.05**	0.70 ± 0.05***	0.67 ± 0.06*
% OHC fold	0%	14%	99.2%	100%
Fold angle (°)	0	4.1 ± 10.3	54.7 ± 14.0***	59.6 ± 10.1
Fold radius (µm)	-	-10.9 ± 2.9	-3.8 ± 2.2*	-2.5 ± 1.0**
% OHC base	0%	36%	100%	100%
Lobes radius (µm)	-	2.4 ± 0.2	2.0 ± 0.2**	1.8 ± 0.2***
OHC1	n=54	n=21	n=125	n=23
Area (µm²)	36.2 ± 3.3	31.5 ± 2.0***	20.6 ± 2.4***	15.9 ± 1.6***
Perimeter (µm)	21.9 ± 1.07	21.3 ± 0.8*	18.9 ± 1.1***	17.2 ± 0.7***
Convexity ratio	1.00 ± 0.00	0.98 ± 0.03*	0.87 ± 0.06***	0.84 ± 0.06*
Ratio 4π A/P²	0.95 ± 0.02	0.88 ± 0.05**	0.72 ± 0.04***	0.68 ± 0.05**
% OHC fold	0	14%	96.8%	95.7%
Fold angle (°)	0	5.1 ± 9.1˙	49.5 ± 19.0***	47.9 ± 13.8
Fold radius (µm)	-	-15.5 ± 2.5	-4.9 ± 3.0*	-3.1 ± 1.5**
% OHC base	2%	52%	100%	100%
Lobes radius (µm)	2.7 ± 0.1	2.3 ± 0.1	1.9 ± 0.2***	1.8 ± 0.2**
IHC	n=44	n=21	n=107	n=23
Area (µm²)	54.5 ± 7.71	43.1 ± 7.7**	34.0 ± 8.4**	29.2 ± 3.0**
Perimeter (µm)	27.0 ± 1.88	24.8 ± 2.3**	22.8 ± 1.9*	20.7 ± 0.9***
Convexity ratio	1.00 ± 0.01	0.99 ± 0.02	0.96 ± 0.08**	0.98 ± 0.02*
Ratio 4π A/P²	0.94 ± 0.02	0.88 ± 0.06**	0.81 ± 0.10**	0.85 ± 0.04**

Fig. 2. Reshaping of hair cell apical circumference during postnatal development. (**A**) ZO1-immunolabeling of organs of Corti from P1 to P21 mice. Asterisks denote the OHC rows. Note the reduction in the width of the epithelium along the neural-abneural axis from P1 to P7 at the cochlear base and middle, and the non-convex apical circumference of OHCs from P4, P5 and P7 onwards at the cochlear base, middle and apex, respectively. (**B**) Mean contours and morphological parameters quantifying shape changes in the hair cell apical circumferences at the cochlear base. For each stage, samples of 19-126 contours were extracted from 5-28 confocal images acquired in 2-4 cochleas and were subsequently aligned and averaged. The resulting mean contours are plotted on the left (solid curves) for the various hair cell rows, before (P1, P3) and after (P5, P7.5) the transition. The extracted contours show remarkably little cell-to-cell variation at a given developmental stage (dashed lines represent ± 1 standard deviation (s.d.) of the contour distance to center). Each plotted green segment represents the contour second derivative vector (pointing in the direction of the curvature of the contour, see Materials and methods), locally averaged (Gaussian weighted average with an s.d. of 18°, or 5% of 360°) around the point considered and scaled for display. The inverse of the norm of this vector represents a local average of the radius of the osculating circle of the contour, which we refer to as the local-averaged curvature radius. Geometric parameters describing the shapes of the contours, as well as numbers of averaged contours, are given in the table. Note the marked reductions of the apical surface area and perimeter of both OHCs and IHCs between P3 and P5. The OHC fold angle is defined as the polar angle made by the two inflexion points delimiting the negative curvature region (dashed lines originating from the OHC contour centers at P5 and P7.5; see also Fig. S2A in the supplementary material). The formation of the OHC lobes can be detected as early as P3 by a flattening of the cell circumference on its neural side. A given OHC was considered to have a flattened base if on the neural side of the detected contour (defined as the region situated below the center), the ratio of minimum to maximum curvature (K_{min}/K_{max}) did not exceed +10%. When this was the case, two laterally symmetric points of maximum curvature delimited the base on the neural side. The OHC lobe radius was defined as the mean of the local-averaged curvature radii of these two points (for illustration, see schema in Fig. S2B in the supplementary material). A region of negative curvature was considered present in the OHC contour if (1) the OHC fold angle was >18° and (2) the ratio K_{min}/K_{max} on the neural contour side was less than –10%. In OHCs fulfilling these conditions, the negative curvature region was typically centred on the point of maximum negative curvature at the neural side. The fold radius is defined as the (negative) local-averaged curvature radius at this point (see Fig. S2B in the supplementary material). The above criteria provided convenient means for sampling from the observed continuous distribution of contour shapes displayed by the OHC circumference. Scale bars: 10 µm in A.

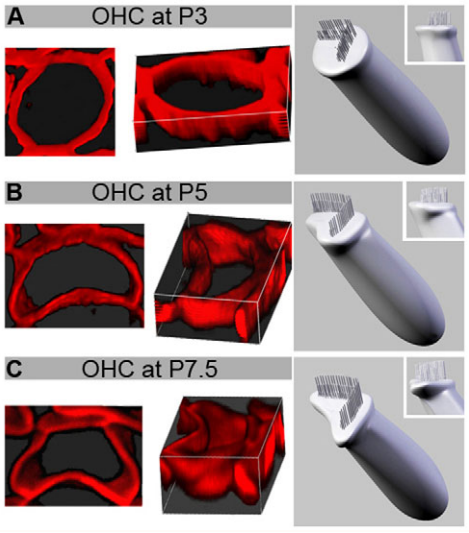

Fig. 3. Three-dimensional reconstructions of ZO1-labeled OHCs from confocal stacks acquired at the cochlear base at postnatal days 3, 5 and 7.5. (**A-C**) For each triptych, the left panel shows a top view of the 3D-apical OHC reconstruction, the middle panel shows a perspective view of this reconstruction and the right panel shows a 3D model of the corresponding OHC. For the reconstructions, an OHC from the second row was selected at each stage (P3, P5 and P7.5 in A, B and C, respectively). The cell selected at P3 had not yet developed a flattened base on its neural side.

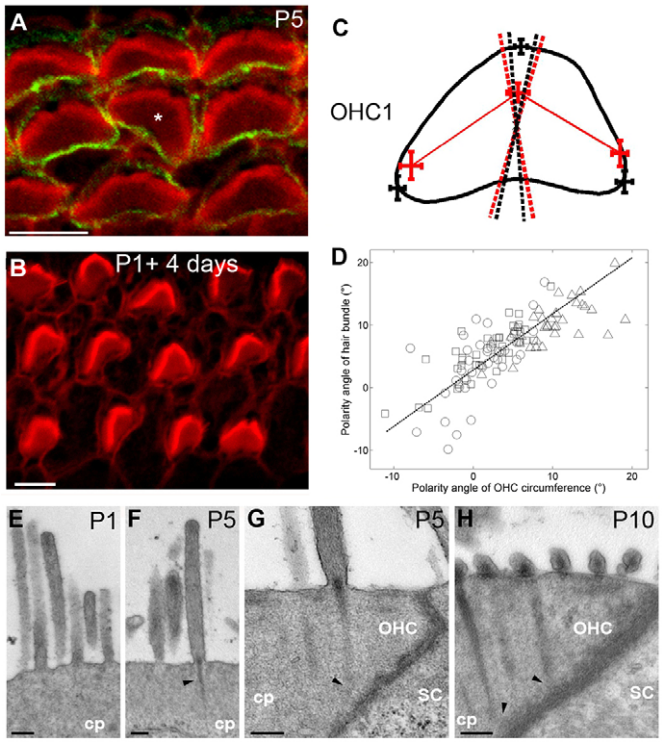

Fig. 4. Correlation between the OHC apical circumference and hair bundle orientations. (**A**) Example of an OHC misaligned with respect to the neural-abneural axis (asterisk) in a P5 cochlea. The hair bundle V-shape (phalloidin-staining of actin filaments in red) remains superimposed to the triangular cell contour shape (ZO1 staining in green). (**B**) Phalloidin staining of a P1 mouse cochlea maintained for 4 days in organotypic culture. Note the persisting match between the orientations of the hair bundle and of the OHC apical circumference. (**C**) Measurement of the polarity angles of the hair bundle and of the OHC apical circumference. The black contour plotted for reference is the average of 37 ZO1-extracted OHC contours from the first row in the same cochlea. A triangle inscribed into the OHC apical circumference was defined, whose base was formed by the two points of maximum curvature marking the positions of the OHC lobes, and whose vertex was the contour point situated abneurally on the bilateral symmetry axis of the contour (black and red crosses indicate 1 s.d.). Similarly, we assigned a triangle to the F-actin-labeled hair bundle (red crosses), with the base formed by the ends of its two arms, and vertex at the hair bundle vertex. The polarity angles of the hair bundle and of the OHC contour, defined as the angles made by the symmetry axes of their respective ascribed triangles relative to the neural-abneural axis, vary over similar ranges indicated by the red and black dashed axes, respectively. (**D**) Plot of the OHC hair bundle polarity angle against the polarity angle of the OHC apical circumference. These two angles display a range of variation of about 20° and a correlation coefficient of 0.78 (n=114 OHCs at the cochlear base). Circles, squares and triangles correspond to cells from OHC row 1, 2 and 3, respectively. (**E-H**) Transmission electron micrograph of OHCs from P1, P5 and P10 mice (vertical ultrathin sections), showing the appearance of rootlets and their connections with the apical junctional complex (AJC). (E) At P1, stereocilia erect vertically above the cuticular plate (cp) but rootlets are not detected. (F) In P5 OHCs from the cochlear apex, stereocilia rootlets are present (arrowhead) but never project to the AJC. (G) At the P5 cochlear base where the OHC lateral lobes are developed, rootlets (arrowhead) project to the junctions. (H) At P10, multiple connections between the rootlets and junctions can be seen in the OHC lobes (arrowheads) throughout the cochlea (here in the middle turn). SC, supporting cell. Scale bars: 5 µm in A,B; 0.2 µm in E-H.

structures included the rare cases in which the axis of symmetry of an OHC hair bundle is strongly misoriented with respect to the neural-abneural planar polarity axis of the normal sensory epithelium (Fig. 4A). Likewise, in organotypic cultures, where planar cell polarity is not as strictly defined, the OHC apical circumferences and hair bundles still matched in their orientations (Fig. 4B). We took advantage of the small variations (up to 20°) in the orientations of OHC bundles with respect to the neural-abneural axis in the P5 cochlea, to assess a possible correlation between the 'polarity angle' of the OHC apical circumference (defined as the angle made by the symmetry axis of the ZO1-extracted contour with the neural-abneural axis) and the polarity angle of the hair bundle (defined similarly from the F-actin staining). We found a significant correlation coefficient of 0.78 between these two angles (n=114 OHCs at the basal turn; Fig. 4C,D). In addition, the vertex of the hair bundle and its lateral extremities had positions relative to the OHC apical circumference that varied within a range of about 0.3 µm, comparable to the stereocilia diameter and probably reflecting measurement errors (see Fig. S4 in the supplementary material).

These observations suggest that internal cortical forces establish and maintain precise alignment between the hair bundle and the apical circumference in OHCs. Because stereocilia of OHCs have been shown to establish physical contacts with the AJC via their rootlets (which anchor stereocilia to the cuticular plate) (Furness et al., 2008), we proceeded to examine when such contacts develop in the mouse. At P1, no stereociliary rootlet was detected by transmission electron microscopy carried out on ultrathin cross-sections of wild-type cochleas, whereas at P5, rootlets were present in all OHCs (Fig. 4E-G). On this day, rootlets that originated in the most lateral stereocilia of the hair bundle were observed to project to the AJC in the lobes region (Fig. 4G), but only in OHCs from the cochlear base that had already undergone their apical shape

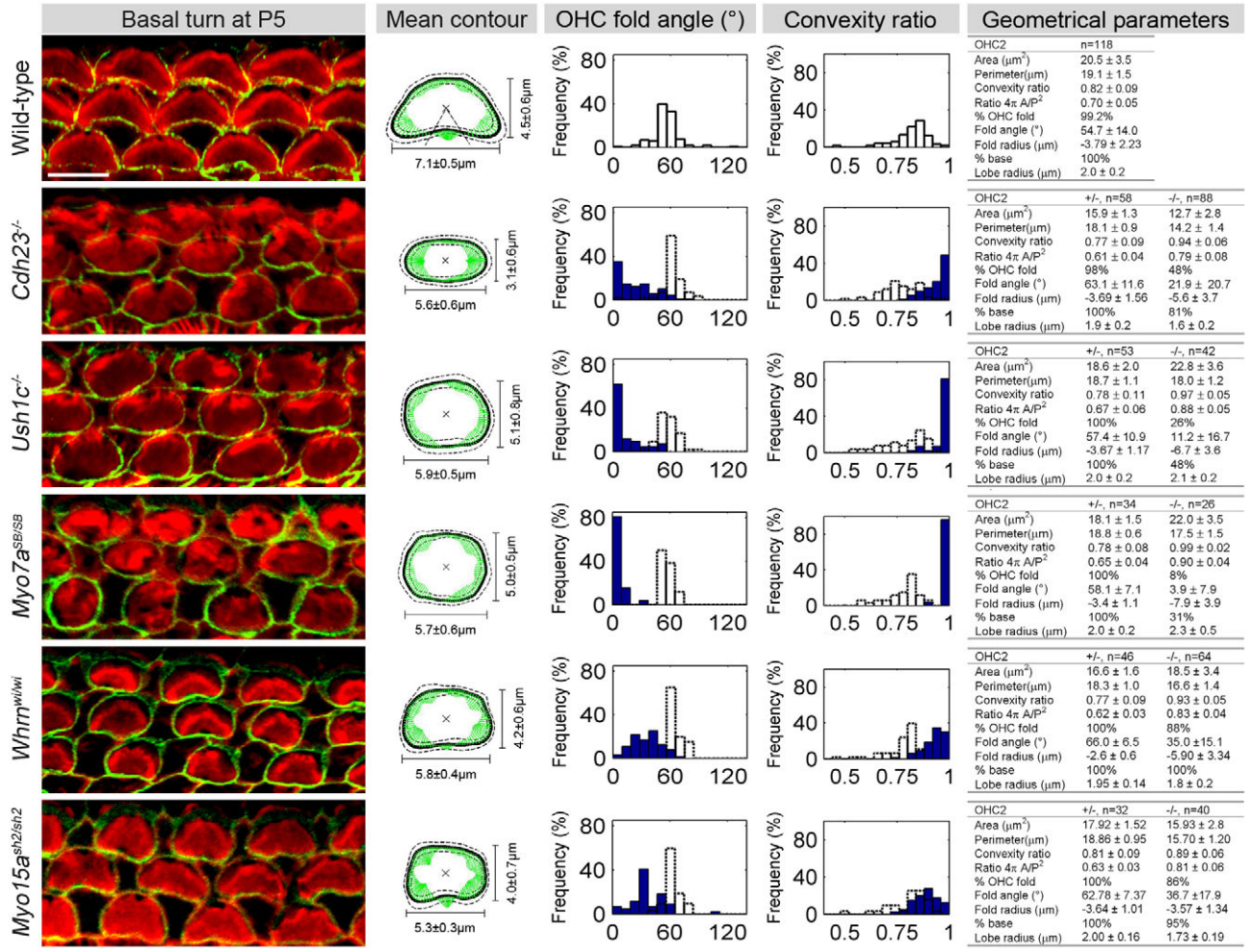

Fig. 5. Reshaping of the OHC apical circumference crucially depends on hair bundle integrity. Columns are described from left to right. Column 1: Organs of Corti from a P5 wild-type mouse and five different mutants with defective hair bundle morphogenesis, namely *Cdh23*$^{-/-}$, *Ush1c*$^{-/-}$, *Myo7a*$^{4626SB/4626SB}$ (abbreviated *Myo7a*$^{SB/SB}$), *Whrn*$^{wi/wi}$ and *Myo15a*$^{sh2/sh2}$, were double-stained with an anti-ZO1 antibody (green) and TRITC-conjugated phalloidin to label actin filaments (red). Column 2: OHC apical contours extracted, averaged and analyzed using our software. Mean contours are shown for the wild-type and mutant mice. Line styles and colors are as in Fig. 2B. Columns 3 and 4: Distributions of the OHC fold angle and the convexity ratio of the extracted contours in the wild-type and mutant mice. Blue-filled and dashed bar graphs are for homozygote and heterozygote mutants, respectively. Column 5: Averaged geometric parameters of the extracted contours for wild-type, heterozygote (+/–) and homozygote (–/–) mutant mice. In harmonin-null (*Ush1c*$^{-/-}$) mutants, a majority of OHCs has no detectable negative curvature (0° fold angle), even though a small proportion of OHCs (<30%) displays a small negative curvature region (<25°). The myosin VIIa-defective OHCs, which display the most severe hair bundle defects (Lefèvre et al., 2008), have the most perturbed apical circumference among the mutants studied, with >90% of cells having no detectable negative curvature region and the smallest fraction of cells developing a flattened base (~30%). OHCs from *Cdh23*$^{-/-}$, *Ush1c*$^{-/-}$ and *Myo7a*$^{4626SB/4626SB}$ mutants do not develop lateral lobes, but a flattening occurs in some of these cells on the neural side, making it possible to detect a base (see legend of Fig. 2). The 'lobe radius' in the tables refers to the mean curvature radius of the two symmetric points of maximum curvature delimiting this base. Scale bar: 5 µm.

transition. At P10, multiple connections between stereocilia rootlets and the junctions in the OHC lobes could be observed at the cochlear base and apex (Fig. 4H). Thus, the time course of establishment of these connections parallels the OHC apical circumference reshaping.

The OHC apical circumferential shape transition requires hair bundle integrity

The shape correlations and physical connections between the hair bundle and the apical OHC circumference suggest that the non-convex shape of the latter might be dependent on the integrity of the hair bundle. We thus analyzed the apical circumference of OHCs from various mutant mice with abnormal hair bundle morphogenesis. Myosin VIIa-deficient mice (*Myo7a*$^{4626SB/4626SB}$) (Mburu et al., 1997), harmonin-null engineered mutants (*Ush1c*$^{-/-}$) (Lefèvre et al., 2008) and newly engineered cadherin 23-null mice (*Cdh23*$^{-/-}$; see Materials and methods; see also Fig. S1 in the supplementary material), were first studied. In these mutants, the hair bundles are fragmented from their earliest growing stage (Lefèvre et al., 2008) (Fig. 5 for the *Cdh23*$^{-/-}$ mutant). Myosin VIIa is present throughout the hair cells, whereas cadherin 23, which forms transient fibrous links between growing stereocilia (Lagziel et al., 2005; Michel et al., 2005), and harmonin, a PDZ domain-containing protein that binds to the cytoplasmic regions of these

links (Boeda et al., 2002; Lefèvre et al., 2008; Siemens et al., 2002), are only present in the hair bundle. In all of these mutants, the lateral lobes and the negative curvature did not form at the OHC apical circumference, and the distributions of the OHC fold angle and the convexity ratios at the P5 cochlear base markedly differed from the corresponding distributions in wild-type or heterozygote mutant mice (Kolmogorov-Smirnov's test, $P<10^{-9}$ for both parameters and all three OHC rows; Fig. 5). The fold angle distributions were characterized by a pronounced peak at 0°, indicating that a large proportion of the OHCs had no detectable concavity. Notably, the contour of the cuticular plate also remained convex in the mutant OHCs (Fig. 5; see also Fig. S3B in the supplementary material for a higher magnification view of the double staining against ZO1 and actin in *Cdh23*$^{+/-}$ and *Cdh23*$^{-/-}$ mice). The only developmental change of the OHC circumferential shape observed in these mice was a slight flattening on both their neural and abneural sides at P5 (Fig. 5). Of note, the narrowing down of the reticular lamina along the neural-abneural axis that is observed in wild-type mice occurred in all of these mutants. We next asked whether the OHC apical circumference would also be affected in mouse mutants with anomalies of the hair bundle, but preserving its integrity. In whirlin-deficient mice and myosin XVa-deficient mice (whirler and shaker 2 mutants, respectively), stereocilia are abnormally short (Holme et al., 2002; Probst et al., 1998). In addition, the hair bundle displays a linearized rather than a V-shaped configuration in some of the OHCs from whirler mice (Kikkawa et al., 2005). Whirlin, a PDZ domain-containing protein, and myosin XVa are only present in the hair bundle (Belyantseva et al., 2003; Delprat et al., 2005; Rzadzinska et al., 2004). In these two mutants, most OHCs (>85%) developed a non-convex region on their apical circumference, although less pronounced than in wild-type OHCs (fold angle ~35°). The distributions of their fold angle and convexity ratio differed significantly from those of wild-type and of heterozygote OHCs (Kolmogorov-Smirnov's test, $P<10^{-4}$ for the fold angle, $P<0.05$ for the convexity ratio, all three OHC rows). Notably, these differences were not as marked as in the *Myo7a*$^{4626SB/4626SB}$, *Ush1c*$^{-/-}$ and *Cdh23*$^{-/-}$ mutants. In the few OHCs with linear hair bundles, however, neither the lobes nor the negative curvature in between developed (see Fig. S5 in the supplementary material).

Myosin II, myosin VIIa, Shroom2 and F-actin redistribute asymmetrically during the remodeling of the OHC apical circumference

We next investigated the molecular bases of the OHC apical circumference remodeling. To this end, we searched for a possible concomitant redistribution of cadherin and myosin II isoforms, which have well-established concurring roles in tissue morphogenesis as mediators of apical adhesion and of cortical tension, respectively (Bertet et al., 2004; Classen et al., 2005; Hayashi and Carthew, 2004; Lecuit, 2005; Martin et al., 2009). In addition, mutations in *MYH9* and *MYH14* that encode heavy chains of class II non-muscle myosins cause hearing impairment in humans (Donaudy et al., 2004; Lalwani et al., 2000; Seri et al., 2003). We first addressed the controversial issue of whether E-cadherin and N-cadherin, which, in the developing organ of Corti, are restricted to the OHC and the IHC epithelial zone, respectively (see Fig. S7 in the supplementary material), disappear from hair cell junctions after the early postnatal period in the mouse (Mahendrasingam et al., 1997; Nunes et al., 2006; Whitlon, 1993). By using either a paraformaldehyde (data not shown) or a methanol fixation procedure (see Fig. S7 in the supplementary material), we found an early cadherin distribution consistent with previous studies (Nunes et al., 2006; Simonneau et al., 2003). By using methanol fixation, we were able to show that N- and E-cadherin persist at the hair cell-supporting cell junctions at P6 and beyond (see Fig. S7 in the supplementary material), thereby confirming earlier observations in the guinea pig (Leonova and Raphael, 1997). Moreover, we found that E-cadherin was nearly homogeneously distributed all along the apical circumference of OHCs and remained so during the reshaping period.

By contrast, changes in the distributions of several cytoskeleton-associated proteins were observed during the OHC apical shape transition, both in the area of the cuticular plate and at the heterotypic junctions between these cells and their supporting cells. First, NMHCII A and NMHCII B, two of the three isoforms of myosin II in mammals (Ivanov et al., 2007), and the active form of their regulatory light chain that contains a phosphorylated serine (Ser19), displayed conspicuous redistributions (Fig. 6A). From being present all along the OHC apical circumference at P1, the NMHCII A staining adopted a polarized distribution at P3 with predominant signals on the neural side and in a patch on the abneural side, but only in the OHCs that already displayed a flattened neural side at this stage. At P4, this cortical staining became excluded from the forming lobes and at P5 its absence from the lobes was almost complete (Fig. 6A). On the abneural side, the patch of increased labeling that was conspicuous at P4 started to appear faint at P5 and, at P7.5, the abneural vertex of the OHC apical circumference appeared NMHCII A-depleted, although not as markedly as were the lobes. Both NMHCII B and the phosphorylated regulatory light chain showed a similar dynamic redistribution (see Fig. S6 at P5 in the supplementary material). Second, in view of the known genetic interactions between the myosin II and myosin VIIa genes in *Drosophila* (Todi et al., 2008; Winter et al., 2001), and of the association of myosin VIIa with adherens junction proteins (Etournay et al., 2007; Kussel-Andermann et al., 2000; Sousa et al., 2004), we examined the distribution of myosin VIIa, which is restricted to hair cells in the cochlea. As long as the OHC apical circumference was convex, myosin VIIa remained diffusely distributed throughout the cuticular plate (Fig. 6A). At P3, myosin VIIa displayed a more intense staining in the neural region of the cuticular plate of flattened OHCs but not of the circular ones. Thereafter, its staining pattern became strongest in the forming lobes, where it became segregated at P5 and persisted at P7.5 (Fig. 6A). Third, we also studied the distribution of F-actin and that of Shroom2, a PDZ domain-containing protein of tight junctions, which directly interacts with myosin VIIa and binds to F-actin (Etournay et al., 2007). Notably, Shroom proteins have been reported to control the distribution of cytoskeletal proteins during the apical reshaping of epithelial cells (Lee et al., 2009; Nishimura and Takeichi, 2008). At P1, Shroom2 was distributed at all the apical junctions of the reticular lamina but was especially abundant at heterotypic junctions (Fig. 6A) together with F-actin, in agreement with previous results at P2 and P10 (Etournay et al., 2007). Surprisingly, at P3, Shroom2 showed a decrease in its junctional staining in every OHC, circular or not (Fig. 6A), but remained present at the homotypic junctions between supporting cells (not shown). In parallel, a Shroom2 labeling appeared in the cuticular plate lining the neural side of the OHC circumference, whereas no such change was detected in the cytoplasm of supporting cells (not shown). At P4, this staining pattern was replaced by a Shroom2 labeling of the emerging lobes, both at the junctions with supporting cells and in the cuticular plate. At P5, the Shroom2 immunoreactivity increased in the lobes together with the F-actin staining (Fig. 6B), and both distributions became similar to that of

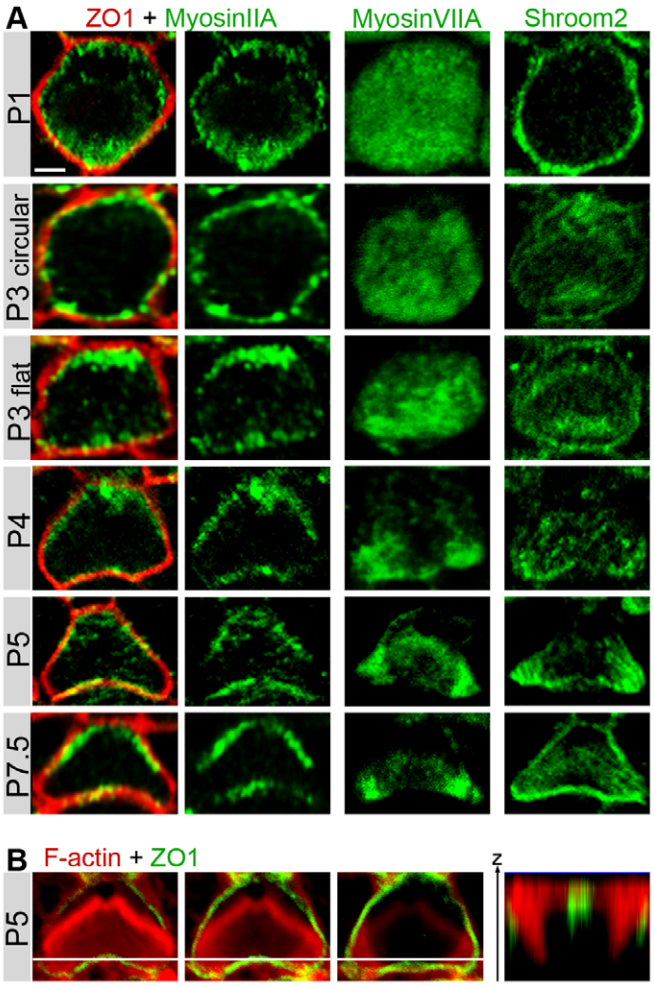

Fig. 6. Redistribution of cell-cortex proteins during OHC apical reshaping. (**A**) Organs of Corti at the base of cochleas from mice aged between P1 and P7.5 were double-stained with the anti-ZO1 monoclonal antibody and the anti-myosin IIA, anti-myosin VIIa or anti-Shroom2 polyclonal antibody. Each panel shows a maximum projection of two adjacent confocal optical sections. The ZO1 immunolabeling, shown only in combination with the myosin IIA staining (first column from the left) was used in each case to control the flatness of the reticular lamina. The second column shows single channel myosin IIA immunostaining. The third and fourth columns show myosin VIIa and Shroom2 immunostaining, respectively. (**B**) Confocal sections at three consecutive levels showing that the lateral arms of the V-shaped hair bundle extend over the F-actin-filled lobes. The right panel shows an orthogonal projection of both F-actin and ZO1 channels from the whole *z*-stack at the level of the horizontal white line. Scale bar: 1 μm.

myosin VIIa at this stage. Strikingly, the Shroom2 staining disappeared from the cuticular plate in the fully developed lobes at P7.5 and adopted a distribution reminiscent of that seen at P1, while F-actin, although abundant in the cuticular plate, no longer showed an accumulation in the lobe subregions.

Redistribution of myosin II, myosin VIIa, Shroom2 and F-actin fails in mouse mutants with abnormal hair bundle morphogenesis

Considering the aforementioned deleterious effect of hair bundle anomalies on the OHC apical circumference reshaping, we next studied the distributions of myosin II, myosin VIIa, Shroom2 and F-actin in P5 mutant mice with hair bundle dysmorphism. In the *Myo7a*$^{4626SB/4626SB}$ and *Cdh23*$^{-/-}$ mutants, we observed that myosin II remained distributed all along the apical circumference (Fig. 7A). In addition, myosin VIIa was diffusely spread in the cuticular plate of the *Cdh23*$^{-/-}$ OHCs (Fig. 7B). Shroom2 remained distributed at cell-cell junctions in the *Myo7a*$^{4626SB/4626SB}$, *Cdh23*$^{-/-}$ and *Ush1c*$^{-/-}$ mutants, and on occasion was seen to localize ectopically in patches close to the OHC circumference (Fig. 7C). In these mutants, F-actin was, however, predominantly present at the OHC neural side. By contrast, the distributions of Shroom2 and F-actin in OHCs from whirler mice, which still develop small lateral lobes, did show an accumulation in the region of the lobes, although it was less pronounced than in wild-type OHCs.

DISCUSSION

We showed that during postnatal development in the mouse, cochlear OHCs acquire a non-convex apical circumference molded to the V-shape of their overlying hair bundle. Strikingly, this remodeling of the OHC apical junctions occurs during the period (between P2 and P12 in mice) that corresponds to the onset of OHC electromotility (Abe et al., 2007; Belyantseva et al., 2000; Zheng et al., 2000).

Which cellular mechanisms are involved in the reshaping of the OHC apical circumference?

The surface of the organ of Corti acquires its organization in rows of sensory cells and supporting cells between embryonic day E14.5 and birth in the mouse by a convergent extension process that is thought to involve the planar cell polarity signaling pathway (Kelly and Chen, 2007; Montcouquiol and Kelley, 2003; Montcouquiol et al., 2003; Yamamoto et al., 2009). This process consists of extension along the cochlear duct accompanied by a thinning of the epithelium, during which cell intercalations occur and cell-cell junctions appear or disappear (Keller et al., 2000; Kelly and Chen, 2007). By contrast, the shape transition described here preserves all existing contacts between neighboring cells. The observed changes in shape of the OHC apical circumference are inconsistent with a passive process driven by minimization of surface energy, which would lead to a convex (typically hexagonal) circumference. Therefore, active mechanisms should participate in these changes. During the period between P1 and P8, the width of the reticular lamina decreases nearly by a factor two at the cochlear base, while, in parallel, the microtubule-filled supporting cells undergo rearrangements at and under the surface of the organ of Corti [notably, the bases of the inner and outer pillar cells separate from each other to form the tunnel of Corti (Whitlon et al., 1999)]. One might argue that the resulting compression of the OHC apical circumference against the developing cuticular plate, which is presumably reinforced in the region of the hair bundle, could be sufficient to induce the observed non-convexity. Such a scenario, however, would not apply at the cochlear apex where the reticular lamina width does not decrease, but rather increases during the same period (Burda and Branis, 1988). Moreover, a shape transition mechanism driven primarily by such ‘external’ epithelial forces acting on the OHC apical circumferences would not explain the near normal shape of these circumferences in the rare OHCs showing strong polarization defects (Fig. 4A). Consistent with this view, redistributions of myosin II, myosin VIIa, Shroom2 and F-actin during the transition were not observed elsewhere than inside OHCs or at the apical junctions of OHCs with their supporting cells. No obvious change in the staining pattern of these molecules was detected inside supporting cells, nor at the IHCs. Thus, our results

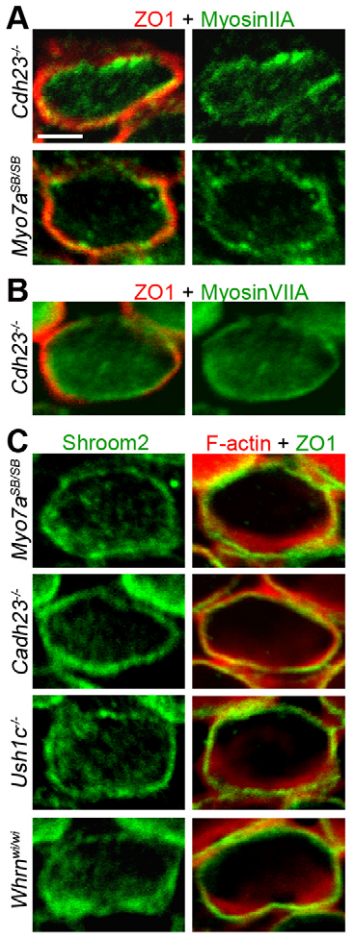

Fig. 7. Distribution of cell-cortex proteins in P5 mutant mice with hair-bundle defects. Wholemount organs of Corti were double-immunostained with the anti-ZO1 monoclonal antibody and the anti-myosin IIA, anti-myosin VIIa or anti-Shroom2 polyclonal antibody, or with TRITC-conjugated phalloidin to label actin filaments. Each confocal acquisition was taken at the cochlear base, where the wild-type shape transition is most pronounced. (**A**) Myosin IIA is present all along the OHC apical circumference in the *Cdh23*$^{-/-}$ and *Myo7a*$^{4626SB/4626SB}$ mice. (**B**) Myosin VIIa is abnormally distributed in the cuticular plate and along the OHC apical circumference in *Cdh23*$^{-/-}$ mice. (**C**) In *Myo7a*$^{4626SB/4626SB}$, *Cdh23*$^{-/-}$ and *Ush1c*$^{-/-}$ mice, Shroom2 and F-actin are abnormally distributed, whereas in *Whrn*$^{wi/wi}$ mice, in which OHC lobes are detectable, Shroom2 and F-actin are still detected within the lobes. Scale bar: 2 μm.

argue in favor of a major role of cortical processes internal to the OHCs in the non-convex reshaping of their apical circumference. However, some of the differences in the circumferential shapes of the three OHC rows might reflect differences in the configuration of their adjacent supporting cells. In particular, at points where the junction between two supporting cells met an OHC, a local outward deformation of the OHC apical circumference could often be observed (see Fig. 2A, images from the cochlear base and middle at P5, P6 and P7). Thus, in OHCs from the first row, part of the variability in the negative curvature of the apical circumference could be ascribed to the variable number (1 or 2) of inner pillar cells that these OHCs contact on their neural side. This suggests that external forces applied by supporting cells can influence the apical circumference of OHCs.

Our analysis of mutant mice with defective hair bundle morphogenesis shows that hair bundle integrity is required for the OHC apical shape transition to occur. The gradual dependency of the OHC apical circumference anomalies on the severity of hair bundle defects supports the notion that the final shape of the AJC circumference is determined by morphogenetic constraints that involve the hair bundle. This raises the question of the nature of the link between the hair bundle and the AJC of OHCs. The observation that the shape of the OHC apical circumference closely delimits that of the cuticular plate implies that one could describe the transition as resulting in the molding of the cuticular plate to the shape of the hair bundle. We further suggest that the development of the lateral lobes is initiated in the cuticular plate. The formation of a circumferential concavity in the cuticular plate also implies that its neural region must be the siege of cytoskeletal reorganization during the transition period (involving presumably plastic deformation and polymerization-depolymerization of the F-actin network). However, the early redistribution of myosin II out of the AJC of the presumptive lobes could also be a triggering event. More work will be required to sort out the causal relationships between these events. At any rate, the anchoring of stereocilia rootlets to the developing cuticular plate provides the most natural path for mechanical interaction between the hair bundle and the AJC. In addition, the present study shows that connections between stereociliary rootlets and junctions form around P5 in mouse OHCs, suggesting that a direct physical hair bundle-AJC coupling is established during the shape transition period. Thus, our results suggest that the constraints imposed by the hair bundle on the reshaping of the OHC apical circumference are primarily of a mechanical nature.

How could the redistribution of cortical proteins orchestrate the apical reshaping of OHCs?

According to Laplace's law, a higher membrane curvature corresponds to a lower membrane tension, or a larger pressure applied across the membrane, or both. The asymmetrical distributions adopted by myosin II and myosin VIIa during and after the OHC apical circumference reshaping are in remarkable agreement with this law. Indeed, the accumulation of myosin VIIa in the inner region of the lobes parallels that of F-actin and of the F-actin bundling protein Shroom2. As Shroom2 stabilizes F-actin at cell-cell junctions and binds to ZO1 (Dietz et al., 2006; Etournay et al., 2007), this suggests a reinforcement of the actin meshwork susceptible to apply large pressures across the membrane of the lobes. Consistent with this view, myosin VIIa, because of its high duty ratio coupled with a high ADP affinity of its F-actin-bound state (Ikebe et al., 2003; Watanabe et al., 2006), has been suggested to mediate the maintenance of tensions exerted on the early transient stereocilia links and the tip-links (Boeda et al., 2002; Hasson and Mooseker, 1997; Kussel-Andermann et al., 2000; Michalski et al., 2009). As for myosin II, its depletion from the lobes is suggestive of a reduced cortical tension in the membrane of this region (Bertet et al., 2004), paralleling the increased pressure across this membrane due to the recruitment of myosin VIIa. We thus hypothesize that, during and after the transition, myosin VIIa generates and maintains an internal set of tensions applied to the developing lobes, while depletion of myosin II would assist the maintenance of a high membrane curvature in this region. The two redistributions could be either triggered in parallel or they could be causally linked. For example, myosin II could redistribute in response to the increased pressure across the membrane of the lobes (Pouille et al., 2009). In either case, the two myosins appear to play complementary roles in the shaping of the OHC lobes, reminiscent of their apparent

complementary roles in the regulation of wing hair number in *Drosophila* that have been previously suggested from genetic studies (Winter et al., 2001).

How does the AJC reshaping of OHCs assist their function in the cochlea?

One role that could be ascribed to the OHC apical shape transition described here relates to the tilting of a large portion of the AJC of OHCs toward the plane of the reticular lamina, due to the formation of the lateral lobes. This tilting is likely crucial for anchoring the apices of OHCs to the surrounding supporting cells within the reticular lamina, thereby permitting the transmission and distribution of potentially large sound-evoked forces at their AJC with minimal membrane shear strain. However, it is for the detection of the very small forces acting on the hair bundles near the hearing threshold that OHCs have an essential role in amplifying the vibrations of the organ of Corti (Fettiplace and Hackney, 2006). Moreover, cochlear amplification is most important at the cochlear base, where the apical shape changes of OHCs are the most pronounced. It has been shown that electromotility forces produced by OHCs along their cell bodies cause deflection of the stereocilia (Kennedy et al., 2006). This mechanism might provide an important route for mechanical feedback contributing to cochlear amplification. What could then be the role of the non-convex apical circumference of OHCs? We propose that the net result of the shape transition is to tighten the mechanical coupling between three structures, namely the OHC basolateral membrane, the AJC formed by the OHC and its supporting cells, and the hair bundle. Owing to the configuration of the OHC hair bundle, which is attached at its tip to the overlying tectorial membrane, forces communicated at the stereocilia bases effectively promote hair bundle deflection (Gueta et al., 2008). By redirecting forces produced by electromotility along the OHC bodies toward the stereocilia bases, this shape could permit small forces to be effectively and locally converted into deflective constraints. In this view, OHCs appear to have evolved a unique morphomechanical solution to cope with the dual mechanical requirements imposed by their amplifier function.

Acknowledgements

We thank S. Chardenoux, E. Bizard, I. Perfettini and O. Alegria-Prévot for technical help; J. Levilliers for help in the preparation of the manuscript; G. Lefèvre for stimulating discussions; the Plate-Forme d'Imagerie Dynamique and the Plate-Forme de Microscopie Ultrastructurale of the Pasteur Institute Imagopole for technical assistance; and the Institut Clinique de la Souris at Illkirch, 67404, France, for help in the generation of the *Cdh23* knockout mice. R.E. and L.L. received fellowships from the Collège de France and the Fondation pour la Recherche Médicale, respectively; R.E. acknowledges a Marie Curie fellowship from the EU 7th Framework Programme (FP7); J.B.M. acknowledges support from the Hugot Foundation of the Collège de France. This work was supported by grants from the Fondation Raymonde et Guy Strittmatter, the Réunica-Prévoyance Group, European Commission FP6 Integrated Project EuroHear (LSHG CT-2004-512063), the A. & M. Suchert-Retina Kontra Blindheit Stiftung and the French National Research Agency.

Competing interests statement

The authors declare no competing financial interests.

Supplementary material

Supplementary material for this article is available at
http://dev.biologists.org/lookup/suppl/doi:10.1242/dev.045138/-/DC1

References

Abe, T., Kakehata, S., Kitani, R., Maruya, S., Navaratnam, D., Santos-Sacchi, J. and Shinkawa, H. (2007). Developmental expression of the outer hair cell motor prestin in the mouse. *J. Membr. Biol.* **215**, 49-56.

Ashmore, J. (2008). Cochlear outer hair cell motility. *Physiol. Rev.* **88**, 173-210.

Belyantseva, I. A., Adler, H. J., Curi, R., Frolenkov, G. I. and Kachar, B. (2000). Expression and localization of prestin and the sugar transporter GLUT-5 during development of electromotility in cochlear outer hair cells. *J. Neurosci.* **20**, RC116.

Belyantseva, I. A., Boger, E. T. and Friedman, T. B. (2003). Myosin XVa localizes to the tips of inner ear sensory cell stereocilia and is essential for staircase formation of the hair bundle. *Proc. Natl. Acad. Sci. USA* **100**, 13958-13963.

Bertet, C., Sulak, L. and Lecuit, T. (2004). Myosin-dependent junction remodelling controls planar cell intercalation and axis elongation. *Nature* **429**, 667-671.

Beurg, M., Fettiplace, R., Nam, J. H. and Ricci, A. J. (2009). Localization of inner hair cell mechanotransducer channels using high-speed calcium imaging. *Nat. Neurosci.* **12**, 553-558.

Boeda, B., El-Amraoui, A., Bahloul, A., Goodyear, R., Daviet, L., Blanchard, S., Perfettini, I., Fath, K. R., Shorte, S., Reiners, J. et al. (2002). Myosin VIIa, harmonin and cadherin 23, three Usher I gene products that cooperate to shape the sensory hair cell bundle. *EMBO J.* **21**, 6689-6699.

Brownell, W. E., Bader, C. R., Bertrand, D. and de Ribaupierre, Y. (1985). Evoked mechanical responses of isolated cochlear outer hair cells. *Science* **227**, 194-196.

Burda, H. and Branis, M. (1988). Postnatal development of the organ of Corti in the wild house mouse, laboratory mouse, and their hybrid. *Hear. Res.* **36**, 97-105.

Classen, A. K., Anderson, K. I., Marois, E. and Eaton, S. (2005). Hexagonal packing of Drosophila wing epithelial cells by the planar cell polarity pathway. *Dev. Cell* **9**, 805-817.

Dallos, P. (1992). The active cochlea. *J. Neurosci.* **12**, 4575-4585.

Dallos, P., Wu, X., Cheatham, M. A., Gao, J., Zheng, J., Anderson, C. T., Jia, S., Wang, X., Cheng, W. H., Sengupta, S. et al. (2008). Prestin-based outer hair cell motility is necessary for mammalian cochlear amplification. *Neuron* **58**, 333-339.

Delprat, B., Michel, V., Goodyear, R., Yamasaki, Y., Michalski, N., El-Amraoui, A., Perfettini, I., Legrain, P., Richardson, G., Hardelin, J.-P. et al. (2005). Myosin XVa and whirlin, two deafness gene products required for hair bundle growth, are located at the stereocilia tips and interact directly. *Hum. Mol. Genet.* **14**, 401-410.

DeRosier, D. J. and Tilney, L. G. (1989). The structure of the cuticular plate, an in vivo actin gel. *J. Cell Biol.* **109**, 2853-2867.

Dietz, M. L., Bernaciak, T. M., Vendetti, F., Kielec, J. M. and Hildebrand, J. D. (2006). Differential actin-dependent localization modulates the evolutionarily conserved activity of Shroom family proteins. *J. Biol. Chem.* **281**, 20542-20554.

Donaudy, F., Snoeckx, R., Pfister, M., Zenner, H. P., Blin, N., Di Stazio, M., Ferrara, A., Lanzara, C., Ficarella, R., Declau, F. et al. (2004). Nonmuscle myosin heavy-chain gene MYH14 is expressed in cochlea and mutated in patients affected by autosomal dominant hearing impairment (DFNA4). *Am. J. Hum. Genet.* **74**, 770-776.

Etournay, R., Zwaenepoel, I., Perfettini, I., Legrain, P., Petit, C. and El-Amraoui, A. (2007). Shroom2, a myosin-VIIa- and actin-binding protein, directly interacts with ZO-1 at tight junctions. *J. Cell Sci.* **120**, 2838-2850.

Fanning, A. S. and Anderson, J. M. (2009). Zonula occludens-1 and -2 are cytosolic scaffolds that regulate the assembly of cellular junctions. *Ann. New York Acad. Sci.* **1165**, 113-120.

Fettiplace, R. and Hackney, C. M. (2006). The sensory and motor roles of auditory hair cells. *Nat. Rev. Neurosci.* **7**, 19-29.

Frank, G., Hemmert, W. and Gummer, A. W. (1999). Limiting dynamics of high-frequency electromechanical transduction of outer hair cells. *Proc. Natl. Acad. Sci. USA* **96**, 4420-4425.

Fritzsch, B., Pauley, S. and Beisel, K. W. (2006). Cells, molecules and morphogenesis: the making of the vertebrate ear. *Brain Res.* **1091**, 151-171.

Frolenkov, G. I., Belyantseva, I. A., Friedman, T. B. and Griffith, A. J. (2004). Genetic insights into the morphogenesis of inner ear hair cells. *Nat. Rev. Genet.* **5**, 489-498.

Furness, D. N., Mahendrasingam, S., Ohashi, M., Fettiplace, R. and Hackney, C. M. (2008). The dimensions and composition of stereociliary rootlets in mammalian cochlear hair cells: comparison between high- and low-frequency cells and evidence for a connection to the lateral membrane. *J. Neurosci.* **28**, 6342-6353.

Goodyear, R. J., Marcotti, W., Kros, C. J. and Richardson, G. P. (2005). Development and properties of stereociliary link types in hair cells of the mouse cochlea. *J. Comp. Neurol.* **485**, 75-85.

Gueta, R., Barlam, D., Shneck, R. Z. and Rousso, I. (2008). Sound-evoked deflections of outer hair cell stereocilia arise from tectorial membrane anisotropy. *Biophys. J.* **94**, 4570-4576.

Gulley, R. L. and Reese, T. S. (1976). Intercellular junctions in the reticular lamina of the organ of Corti. *J. Neurocytol.* **5**, 479-507.

Hasson, T. and Mooseker, M. S. (1997). The growing family of myosin motors and their role in neurons and sensory cells. *Curr. Opin. Neurobiol.* **7**, 615-623.

Hayashi, T. and Carthew, R. W. (2004). Surface mechanics mediate pattern formation in the developing retina. *Nature* **431**, 647-652.

Holley, M. C. and Ashmore, J. F. (1990). Spectrin, actin and the structure of the cortical lattice in mammalian cochlear outer hair cells. *J. Cell Sci.* **96**, 283-291.

Holme, R. H., Kiernan, B. W., Brown, S. D. and Steel, K. P. (2002). Elongation of hair cell stereocilia is defective in the mouse mutant whirler. *J. Comp. Neurol.* **450**, 94-102.
Hudspeth, A. J. (1989). How the ear's works work. *Nature* **341**, 397-404.
Ikebe, M., Inoue, A., Nishikawa, S., Homma, K., Tanaka, H., Iwane, A. H., Katayama, E., Ikebe, R. and Yanagida, T. (2003). Motor function of unconventional myosin. *Adv. Exp. Med. Biol.* **538**, 143-156; discussion 157.
Ivanov, A. I., Bachar, M., Babbin, B. A., Adelstein, R. S., Nusrat, A. and Parkos, C. A. (2007). A unique role for nonmuscle myosin heavy chain IIA in regulation of epithelial apical junctions. *PLoS One* **2**, e658.
Iwasa, K. H. and Adachi, M. (1997). Force generation in the outer hair cell of the cochlea. *Biophys. J.* **73**, 546-555.
Karavitaki, K. D. and Mountain, D. C. (2007). Imaging electrically evoked micromechanical motion within the organ of Corti of the excised gerbil cochlea. *Biophys. J.* **92**, 3294-3316.
Keller, R., Davidson, L., Edlund, A., Elul, T., Ezin, M., Shook, D. and Skoglund, P. (2000). Mechanisms of convergence and extension by cell intercalation. *Philos. Trans. R. Soc. Lond. B Biol. Sci.* **355**, 897-922.
Kelly, M. and Chen, P. (2007). Shaping the mammalian auditory sensory organ by the planar cell polarity pathway. *Int. J. Dev. Biol.* **51**, 535-547.
Kennedy, H. J., Evans, M. G., Crawford, A. C. and Fettiplace, R. (2006). Depolarization of cochlear outer hair cells evokes active hair bundle motion by two mechanisms. *J. Neurosci.* **26**, 2757-2766.
Kikkawa, Y., Mburu, P., Morse, S., Kominami, R., Townsend, S. and Brown, S. D. (2005). Mutant analysis reveals whirlin as a dynamic organizer in the growing hair cell stereocilium. *Hum. Mol. Genet.* **14**, 391-400.
Kussel-Andermann, P., El-Amraoui, A., Safieddine, S., Nouaille, S., Perfettini, I., Lecuit, M., Cossart, P., Wolfrum, U. and Petit, C. (2000). Vezatin, a novel transmembrane protein, bridges myosin VIIA to the cadherin-catenins complex. *EMBO J.* **19**, 6020-6029.
Lagziel, A., Ahmed, Z. M., Schultz, J. M., Morell, R. J., Belyantseva, I. A. and Friedman, T. B. (2005). Spatiotemporal pattern and isoforms of cadherin 23 in wild type and waltzer mice during inner ear hair cell development. *Dev. Biol.* **280**, 295-306.
Lalwani, A. K., Goldstein, J. A., Kelley, M. J., Luxford, W., Castelein, C. M. and Mhatre, A. N. (2000). Human nonsyndromic hereditary deafness DFNA17 is due to a mutation in nonmuscle myosin MYH9. *Am. J. Hum. Genet.* **67**, 1121-1128.
Lecuit, T. (2005). Adhesion remodeling underlying tissue morphogenesis. *Trends Cell Biol.* **15**, 34-42.
Lee, C., Le, M. P. and Wallingford, J. B. (2009). The shroom family proteins play broad roles in the morphogenesis of thickened epithelial sheets. *Dev. Dyn.* **238**, 1480-1491.
Lefèvre, G., Michel, V., Weil, D., Lepelletier, L., Bizard, E., Wolfrum, U., Hardelin, J.-P. and Petit, C. (2008). A core cochlear phenotype in USH1 mouse mutants implicates fibrous links of the hair bundle in its cohesion, orientation and differential growth. *Development* **135**, 1427-1437.
Legendre, K., Safieddine, S., Kussel-Andermann, P., Petit, C. and El-Amraoui, A. (2008). alphaII-betaV spectrin bridges the plasma membrane and cortical lattice in the lateral wall of the auditory outer hair cells. *J. Cell Sci.* **121**, 3347-3356.
Leonova, E. V. and Raphael, Y. (1997). Organization of cell junctions and cytoskeleton in the reticular lamina in normal and ototoxically damaged organ of Corti. *Hear. Res.* **113**, 14-28.
Mahendrasingam, S., Katori, Y., Furness, D. N. and Hackney, C. M. (1997). Ultrastructural localization of cadherin in the adult guinea-pig organ of Corti. *Hear. Res.* **111**, 85-92.
Mammano, F. and Ashmore, J. F. (1993). Reverse transduction measured in the isolated cochlea by laser Michelson interferometry. *Nature* **365**, 838-841.
Martin, A. C., Kaschube, M. and Wieschaus, E. F. (2009). Pulsed contractions of an actin-myosin network drive apical constriction. *Nature* **457**, 495-499.
Mburu, P., Liu, X. Z., Walsh, J., Saw, D., Jr, Cope, M. J., Gibson, F., Kendrick-Jones, J., Steel, K. P. and Brown, S. D. (1997). Mutation analysis of the mouse myosin VIIA deafness gene. *Genes Func.* **1**, 191-203.
Michalski, N., Michel, V., Caberlotto, E., Lefevre, G. M., van Aken, A. F., Tinevez, J. Y., Bizard, E., Houbron, C., Weil, D., Hardelin, J. P. et al. (2009). Harmonin-b, an actin-binding scaffold protein, is involved in the adaptation of mechanoelectrical transduction by sensory hair cells. *Pflugers Arch.* **459**, 115-130.
Michel, V., Goodyear, R. J., Weil, D., Marcotti, W., Perfettini, I., Wolfrum, U., Kros, C. J., Richardson, G. P. and Petit, C. (2005). Cadherin 23 is a component of the transient lateral links in the developing hair bundles of cochlear sensory cells. *Dev. Biol.* **280**, 281-294.
Montcouquiol, M. and Kelley, M. W. (2003). Planar and vertical signals control cellular differentiation and patterning in the mammalian cochlea. *J. Neurosci.* **23**, 9469-9478.
Montcouquiol, M., Rachel, R. A., Lanford, P. J., Copeland, N. G., Jenkins, N. A. and Kelley, M. W. (2003). Identification of Vangl2 and Scrb1 as planar polarity genes in mammals. *Nature* **423**, 173-177.
Nishimura, T. and Takeichi, M. (2008). Shroom3-mediated recruitment of Rho kinases to the apical cell junctions regulates epithelial and neuroepithelial planar remodeling. *Development* **135**, 1493-1502.
Nowotny, M. and Gummer, A. W. (2006). Nanomechanics of the subtectorial space caused by electromechanics of cochlear outer hair cells. *Proc. Natl. Acad. Sci. USA* **103**, 2120-2125.
Nunes, F. D., Lopez, L. N., Lin, H. W., Davies, C., Azevedo, R. B., Gow, A. and Kachar, B. (2006). Distinct subdomain organization and molecular composition of a tight junction with adherens junction features. *J. Cell Sci.* **119**, 4819-4827.
Pouille, P. A., Ahmadi, P., Brunet, A. C. and Farge, E. (2009). Mechanical signals trigger Myosin II redistribution and mesoderm invagination in *Drosophila* embryos. *Sci. Signal.* **2**, ra16.
Probst, F. J., Fridell, R. A., Raphael, Y., Saunders, T. L., Wang, A., Liang, Y., Morell, R. J., Touchman, J. W., Lyons, R. H., Noben-Trauth, K. et al. (1998). Correction of deafness in shaker-2 mice by an unconventional myosin in a BAC transgene. *Science* **280**, 1444-1447.
Rzadzinska, A. K., Schneider, M. E., Davies, C., Riordan, G. P. and Kachar, B. (2004). An actin molecular treadmill and myosins maintain stereocilia functional architecture and self-renewal. *J. Cell Biol.* **164**, 887-897.
Seri, M., Pecci, A., Di Bari, F., Cusano, R., Savino, M., Panza, E., Nigro, A., Noris, P., Gangarossa, S., Rocca, B. et al. (2003). MYH9-related disease: May-Hegglin anomaly, Sebastian syndrome, Fechtner syndrome, and Epstein syndrome are not distinct entities but represent a variable expression of a single illness. *Medicine* **82**, 203-215.
Siemens, J., Kazmierczak, P., Reynolds, A., Sticker, M., Littlewood-Evans, A. and Muller, U. (2002). The Usher syndrome proteins cadherin 23 and harmonin form a complex by means of PDZ-domain interactions. *Proc. Natl. Acad. Sci. USA* **99**, 14946-14951.
Simonneau, L., Gallego, M. and Pujol, R. (2003). Comparative expression patterns of T-, N-, E-cadherins, beta-catenin, and polysialic acid neural cell adhesion molecule in rat cochlea during development: implications for the nature of Kolliker's organ. *J. Comp. Neurol.* **459**, 113-126.
Somlyo, A. P. and Somlyo, A. V. (2003). Ca^{2+} sensitivity of smooth muscle and nonmuscle myosin II: modulated by G proteins, kinases, and myosin phosphatase. *Physiol. Rev.* **83**, 1325-1358.
Sousa, S., Cabanes, D., El-Amraoui, A., Petit, C., Lecuit, M. and Cossart, P. (2004). Unconventional myosin VIIa and vezatin, two proteins crucial for Listeria entry into epithelial cells. *J. Cell Sci.* **117**, 2121-2130.
Stevenson, B. R., Siliciano, J. D., Mooseker, M. S. and Goodenough, D. A. (1986). Identification of ZO-1: a high molecular weight polypeptide associated with the tight junction (zonula occludens) in a variety of epithelia. *J. Cell Biol.* **103**, 755-766.
Steyger, P. S., Furness, D. N., Hackney, C. M. and Richardson, G. P. (1989). Tubulin and microtubules in cochlear hair cells: comparative immunocytochemistry and ultrastructure. *Hear. Res.* **42**, 1-16.
Thompson, D. W. (1961). *On Growth and Form* (ed. J. T. Bonner). Cambridge: Cambridge University Press.
Todi, S. V., Sivan-Loukianova, E., Jacobs, J. S., Kiehart, D. P. and Eberl, D. F. (2008). Myosin VIIA, important for human auditory function, is necessary for *Drosophila* auditory organ development. *PLoS One* **3**, e2115.
Tomo, I., Boutet de Monvel, J. and Fridberger, A. (2007). Sound-evoked radial strain in the hearing organ. *Biophys. J.* **93**, 3279-3284.
van Netten, S. M., Dinklo, T., Marcotti, W. and Kros, C. J. (2003). Channel gating forces govern accuracy of mechano-electrical transduction in hair cells. *Proc. Natl. Acad. Sci. USA* **100**, 15510-15515.
Wangemann, P. (2006). Supporting sensory transduction: cochlear fluid homeostasis and the endocochlear potential. *J. Physiol.* **576**, 11-21.
Watanabe, S., Ikebe, R. and Ikebe, M. (2006). *Drosophila* myosin VIIA is a high duty ratio motor with a unique kinetic mechanism. *J. Biol. Chem.* **281**, 7151-7160.
Whitlon, D. S. (1993). E-cadherin in the mature and developing organ of Corti of the mouse. *J. Neurocytol.* **22**, 1030-1038.
Whitlon, D. S., Zhang, X., Pecelunas, K. and Greiner, M. A. (1999). A temporospatial map of adhesive molecules in the organ of Corti of the mouse cochlea. *J. Neurocytol.* **28**, 955-968.
Winter, C. G., Wang, B., Ballew, A., Royou, A., Karess, R., Axelrod, J. D. and Luo, L. (2001). *Drosophila* Rho-associated kinase (Drok) links Frizzled-mediated planar cell polarity signaling to the actin cytoskeleton. *Cell* **105**, 81-91.
Yamamoto, N., Okano, T., Ma, X., Adelstein, R. S. and Kelley, M. W. (2009). Myosin II regulates extension, growth and patterning in the mammalian cochlear duct. *Development* **136**, 1977-1986.
Zheng, J., Shen, W., He, D. Z., Long, K. B., Madison, L. D. and Dallos, P. (2000). Prestin is the motor protein of cochlear outer hair cells. *Nature* **405**, 149-155.